Structure
Supplemental Information

The plasticity of molecular interactions governs bacterial microcompartment shell assembly

Basil J. Greber[#], Markus Sutter[#], Cheryl A. Kerfeld[*]

[#] Equal contribution

[*] Lead contact. E-mail: ckerfeld@lbl.gov

This PDF file includes:

Figures S1 to S8
Table S1

Other Supplemental Information for this manuscript includes the following:

Videos S1 and S2

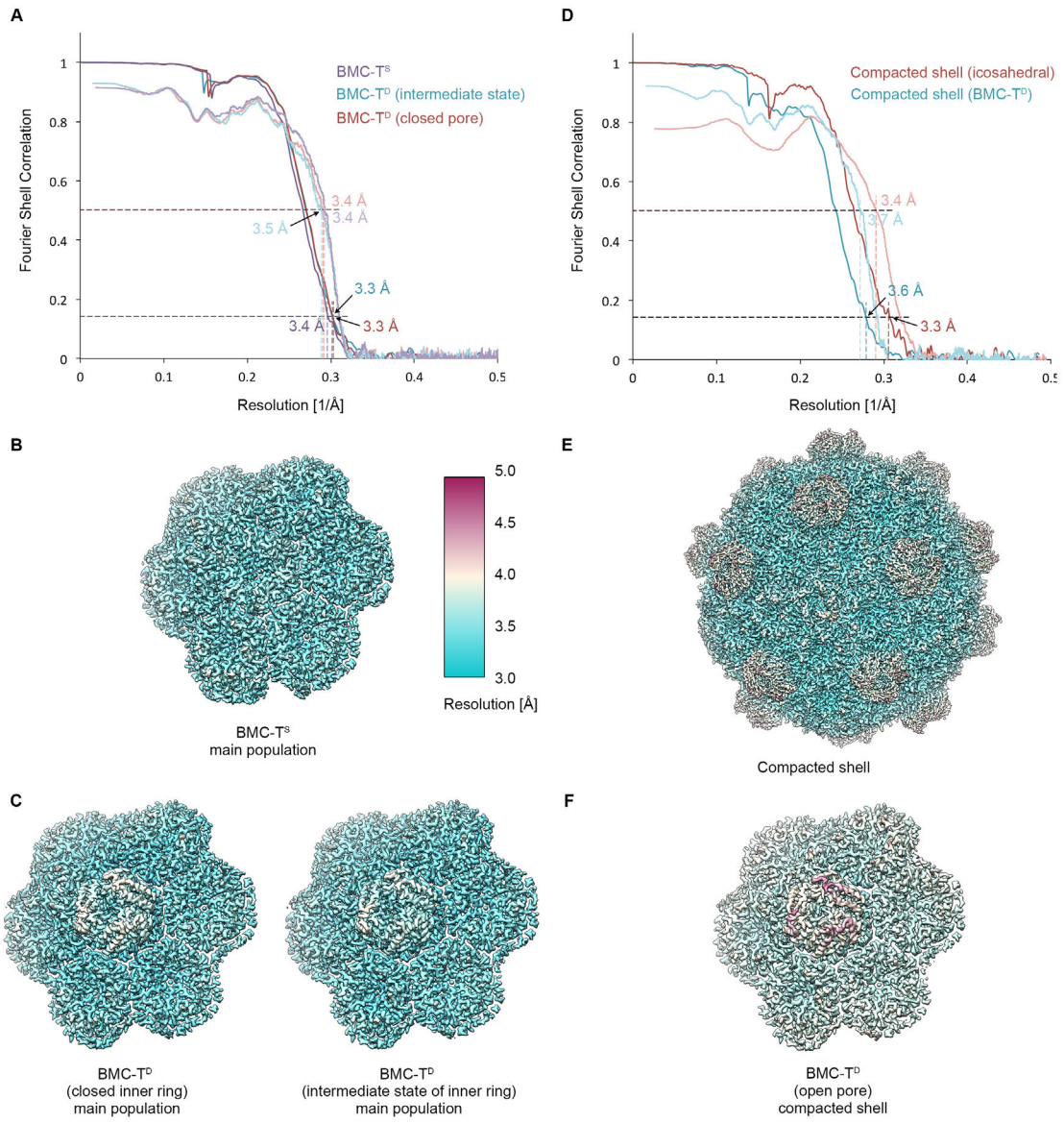

Fig. S1, related to Figs. 5, 6, 8, STAR Methods. FSC and local resolution plots for the cryo-EM maps of BMC-T^S and the maps sorted for conformational states of BMC-T^D and the overall shell.

(**A**) FSC curves computed from fully independent half-maps (gold standard refinement procedure; dark red, blue, and purple) and model vs. map FSC curves (in light red, blue, and purple) for coordinate models refined into the final maps. Resolution estimates are indicated (FSC = 0.143 criterion for FSC curves between half-maps, FSC = 0.5 criterion for model vs. map FSC curves (Rosenthal and Henderson, 2003)).

(**B**) Final post processed (sharpened) map of the BMC-T^S reconstruction colored and filtered according to local resolution.

(**C**) As in (B), but for BMC-T^D reconstruction from the main shell population (closed and intermediate inner pore conformations).

(**D**) As in (A), but for reconstructions based on the compacted shell population.

(**E**) As in (B), but for the icosahedral reconstruction of the compacted shell.

(**F**) As in (B), but for the reconstruction of BMC-T^D in the compacted shell population (open inner pore).

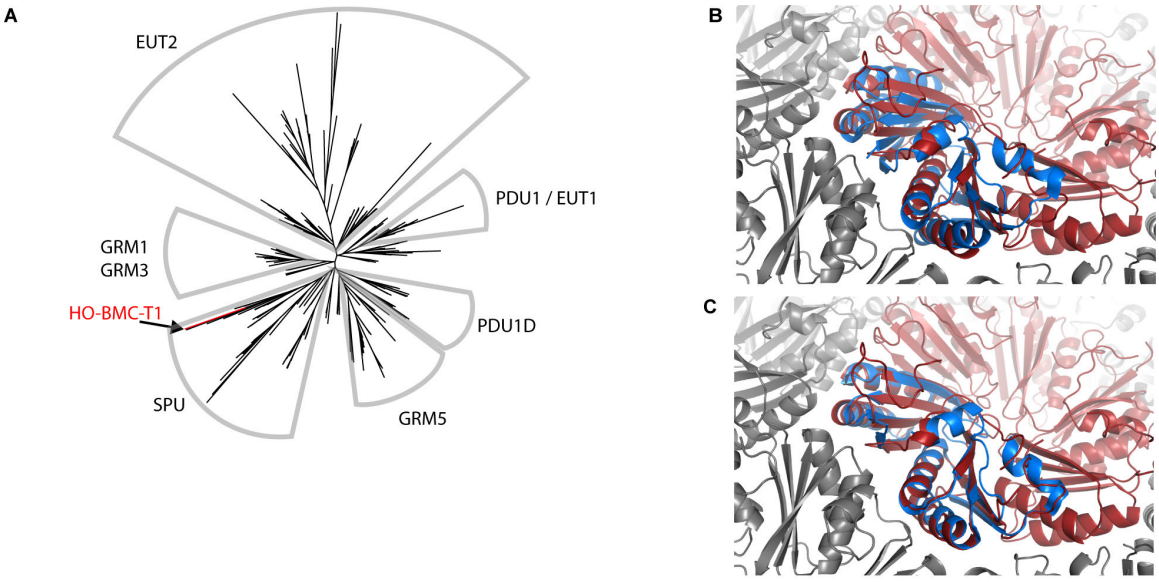

Fig. S2, related to Fig. 5. Structure and sequence analysis of HO-BMC-T^{S}1.

(**A**) Phylogenetic tree of BMC-T^S proteins homologous to HO-BMC-T^{S}1 with BMC type assignments and highlighted HO-BMC-T^{S}1.

(**B**) Comparison of BMC-T^{S}1 (red) with BMC-T^S from *Citrobacter freundii* (PDB ID 3PAC, blue) (Pang et al., 2011) when using a global alignment of the protein chains.

(**C**) Same as A, but aligning the individual domains (residues 2-78 and 79-184 of *C. freundii* BMC-T^S).

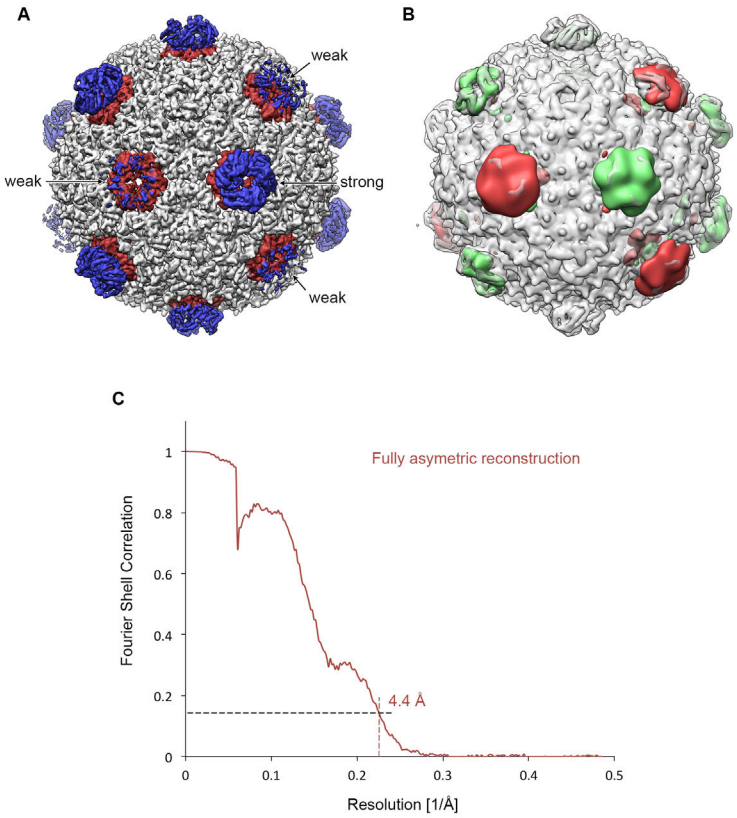

Fig. S3, related to Fig. 7, STAR Methods. Fully asymmetric reconstruction of the HO BMC shell (main population).

(**A**) Cryo-EM map of the BMC shell without use of any symmetry. BMC-T trimers are colored blue (protruding) and brown (embedded). Density for protruding trimers is weak at the indicated positions (arrows).

(**B**) To highlight variable density in BMC-T rings, a difference density was calculated by subtracting the icosahedrally symmetrized map (grey; containing averaged density for the protruding BMC-T^D layers) from the asymmetric map. Positive difference density (indicating predominant presence of BMC-T^D) is shown in green, negative difference density (indicating increased presence of BMC-T^S) is shown in red (orientation as in A).

(**C**) FSC curve for the fully asymmetric reconstruction of the HO BMC shell at 4.4 Å resolution (FSC = 0.143 criterion).

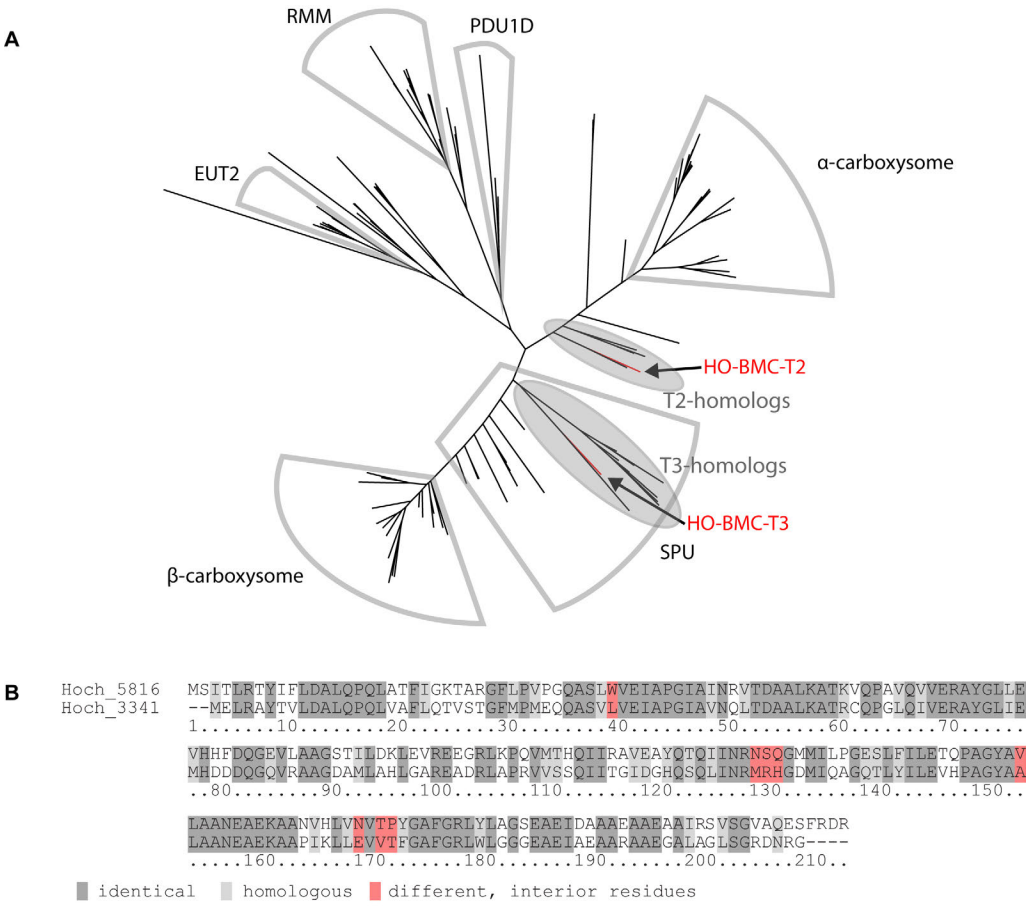

Fig. S4, related to Fig. 8. Sequence analysis of HO-BMC-T^{D}2/T^{D}3

(**A**) Phylogenetic tree of BMC-T^{D} proteins with BMC type assignments and highlighted BMC-T^{D}2 and BMC-T^{D}3 and their closest homologs (shaded).

(**B**) Sequence alignment of BMC-T^{D}2 (Hoch-5816) and BMC-T^{D}3 (Hoch-3341).

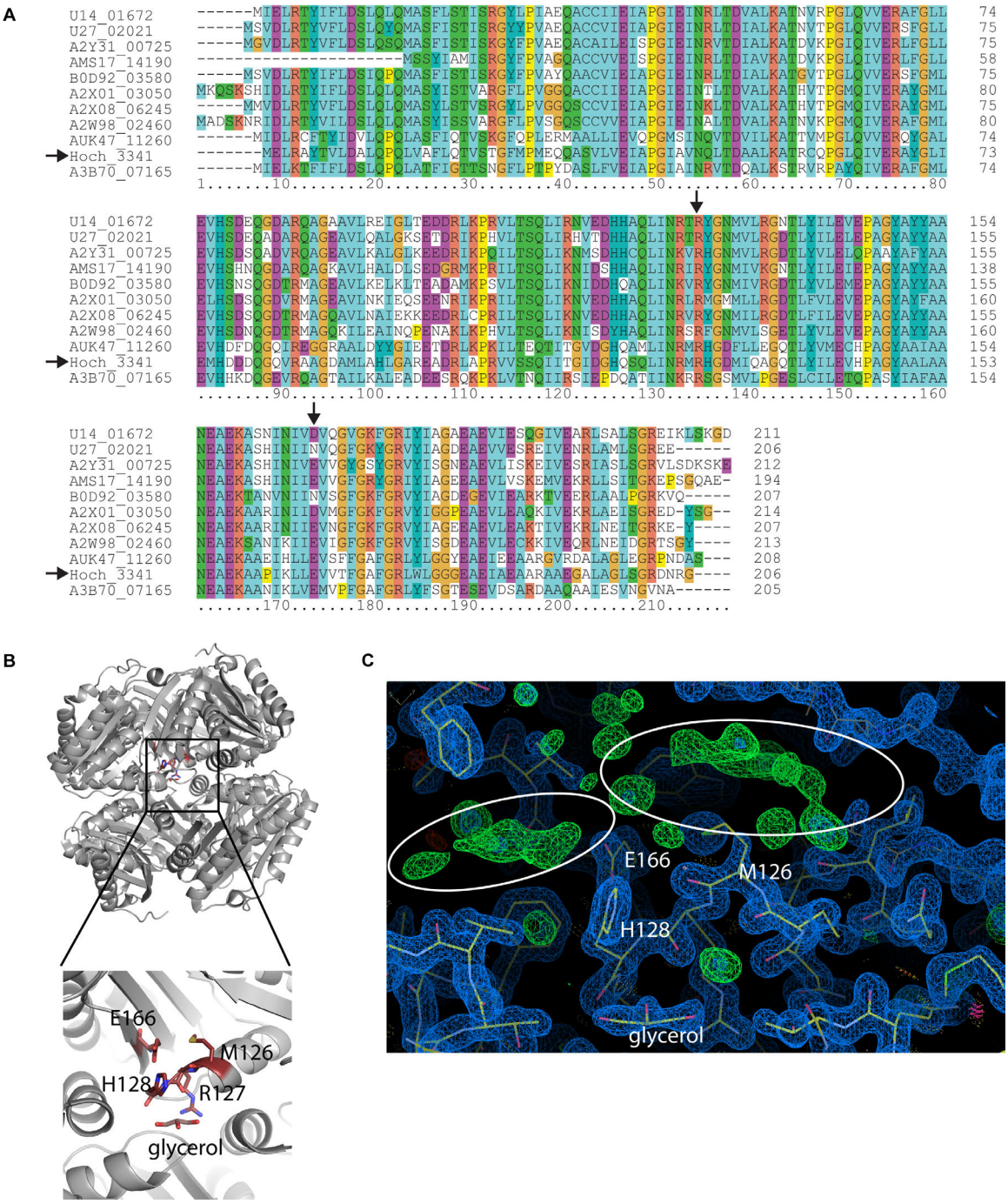

Fig. S5, related to Fig. 8. Analysis of the interior cavity of BMC-T^{D}3.

(**A**) Sequence alignment of the 10 homologs of BMC-T^{D}3 (HO-3341, arrow; as shown in Fig. S4B). Conserved interior residues different from BMC-T^{D}2 are highlighted with arrows.

(**B**) Location of the highlighted residues and a glycerol molecule in the structure of BMC-T^{D}3 shown in overview (left) and close-up view (right).

(**C**) Additional density visible in the crystal structure of BMC-T3. Green: Polder map (Liebschner et al., 2017) of the shown region at 4 rmsd / 0.5 e^-/A^3, blue: 2Fo-Fc map at 2 rmsd / 0.92 e^-/A^3.

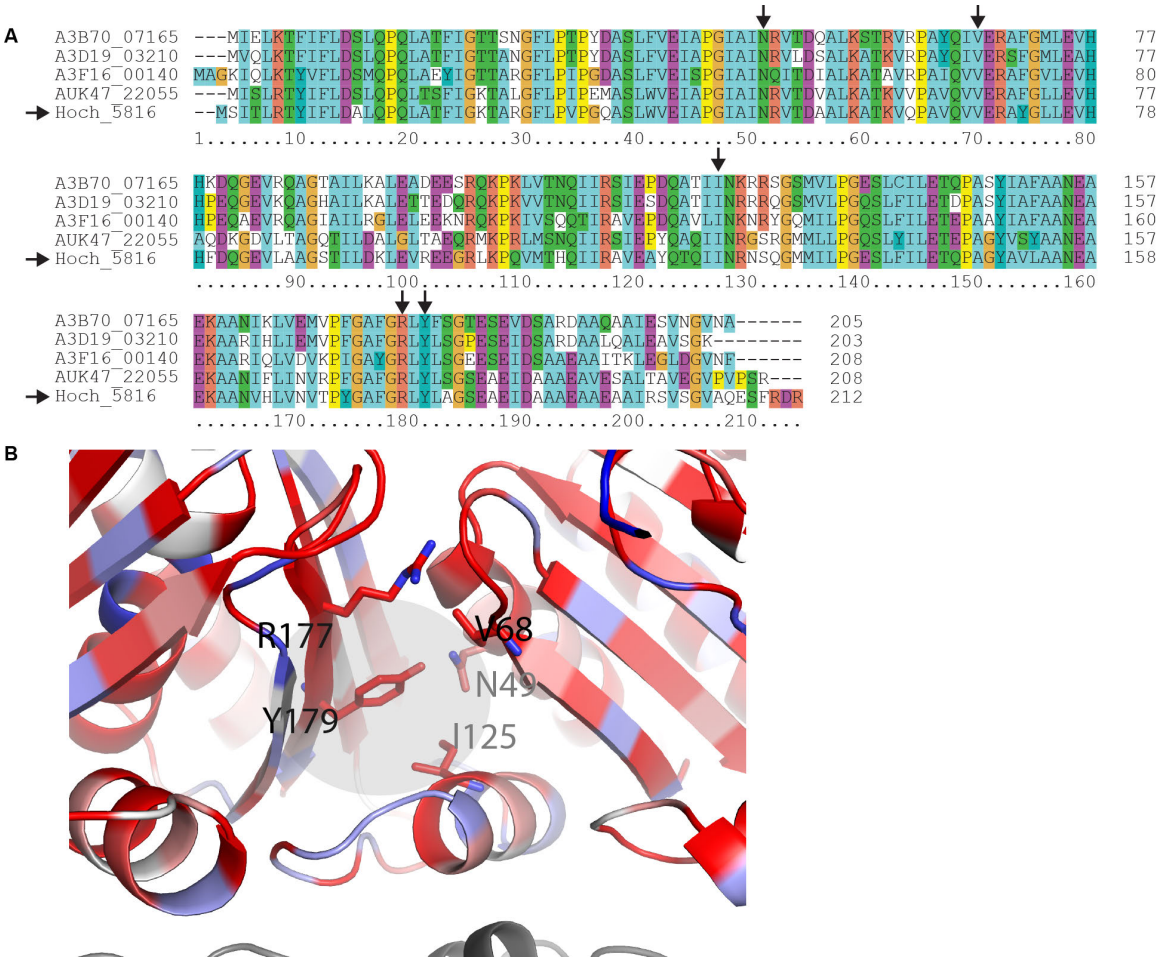

Fig. S6, related to Fig. 8. Analysis of the interior cavity of BMC-T^{D}2.

(**A**) Sequence alignment of the closest homologs of BMC-T^{D}2 (HO-5816, arrow; as shown in Fig. S4B). Coloring by amino acid properties. Conserved interior residues in the pocket between subunits are highlighted with arrows.

(**B**) Location of the conserved pocket between subunits with highlighted residues, coloring by conservation from low (blue) to high conservation (red).

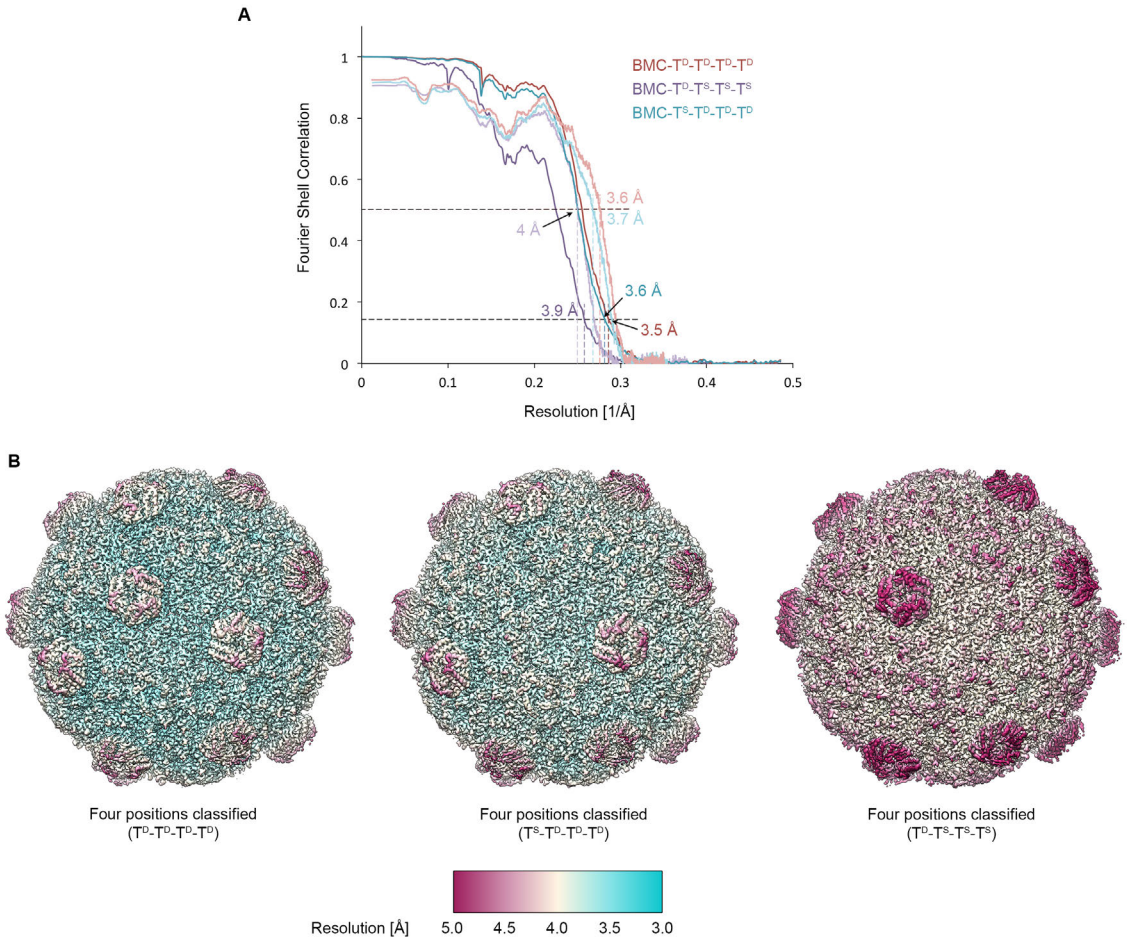

Fig. S7, related to Fig. 9, STAR Methods. FSC and local resolution plots for the cryo-EM maps classified for BMC-T distribution.

(**A**) FSC curves computed from independently refined half-maps (in dark red, blue, and purple) and model vs. map FSC curves (in light red, blue, and purple) for coordinate models refined into the final maps. Resolution estimates are indicated (FSC = 0.143 criterion for FSC curves between half-maps, FSC = 0.5 criterion for model vs. map FSC curves (Rosenthal and Henderson, 2003)).

(**B**) Final post processed (sharpened) maps of three reconstructions sorted for four neighboring BMC-T positions, colored and filtered according to local resolution.

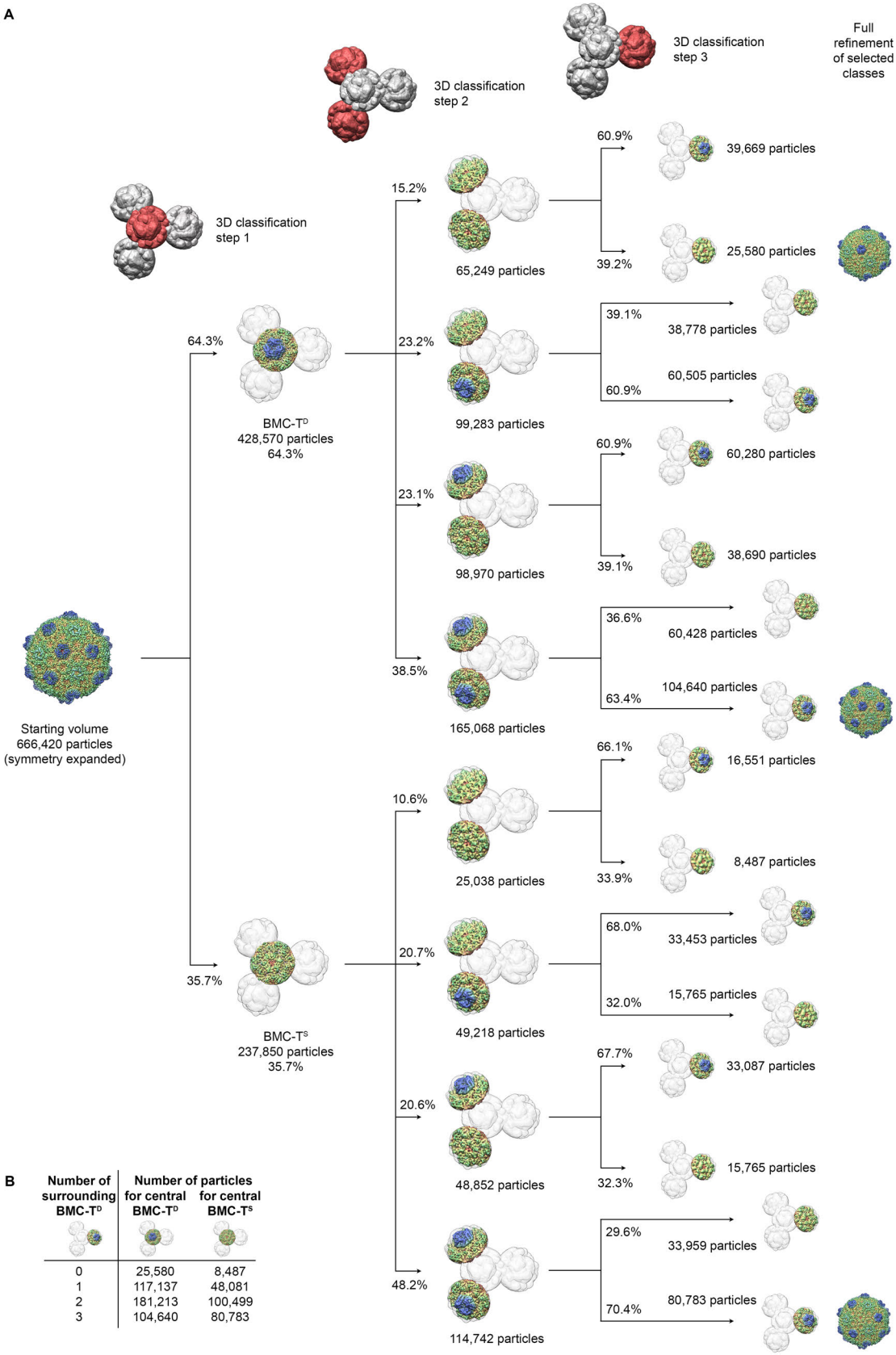
A
3D classification step 1
3D classification step 2
3D classification step 3
Full refinement of selected classes
Starting volume
666,420 particles
(symmetry expanded)
64.3%
BMC-T^D
428,570 particles
64.3%
35.7%
BMC-T^S
237,850 particles
35.7%
15.2%
65,249 particles
60.9%
39,669 particles
39.2%
25,580 particles
23.2%
99,283 particles
39.1%
38,778 particles
60.9%
60,505 particles
23.1%
98,970 particles
60.9%
60,280 particles
39.1%
38,690 particles
38.5%
165,068 particles
36.6%
60,428 particles
63.4%
104,640 particles
10.6%
25,038 particles
66.1%
16,551 particles
33.9%
8,487 particles
20.7%
49,218 particles
68.0%
33,453 particles
32.0%
15,765 particles
20.6%
48,852 particles
67.7%
33,087 particles
32.3%
15,765 particles
48.2%
114,742 particles
29.6%
33,959 particles
70.4%
80,783 particles
B
Number of surrounding BMC-T^D
Number of particles for central BMC-T^D
Number of particles for central BMC-T^S
0 25,580 8,487
1 117,137 48,081
2 181,213 100,499
3 104,640 80,783

Fig. S8 related to Figs. 7, 9, STAR Methods. Classification strategy used for sorting four neighboring BMC-T positions.

(**A**) Three consecutive steps of 3D classification were performed to sort an initial 666,400 particle dataset into 16 classes corresponding to all possible combinations of BMC-T^S and BMC-T^D at four neighboring positions. The masks used are shown at the top; masks used in each step are shown in red, masks not used in this step are shown in grey. Percentages shown above or below arrows refer to the distribution of particles in that specific classification step (not percentage of total particles). Selected classes were subjected to full 3D refinement. The resulting 3D volumes are shown on the right and are discussed further in the text.

(**B**) Summary of the distribution of particles resulting from the classification in (A), grouped by the number of peripheral BMC-T^D building blocks.

Table S1, related to Figs. 2, 3, 5, 6, 8, 9, S1, S7. Data collection, map and model refinement, model validation.

	Large Shell (main population)	Compacted Shell	BMC-T^S large shell	BMC-T^D large shell closed inside	BMC-T^D large shell widened inside	BMC-T^D small shell open inside	Large shell C1 refinement	Four positions: BMC-$T^DT^ST^ST^S$	Four positions: BMC-$T^DT^DT^DT^D$	Four positions: BMC-$T^ST^DT^DT^D$
Accession codes										
Map (EMDB)	EMD-9309	EMD-9310	EMD-9311	EMD-9307	EMD-9308	EMD-9312	EMD-9296	EMD-9314	EMD-9313	EMD-9315
Coordinates (PDB)	6MZX	6MZY	6N06	6MZU	6MZV	6N07	-	6N0F	6N09	6N0G
Data collection										
Microscope	FEI Titan low-base									
Voltage (kV)	300									
Detector	Gatan K2 Summit									
Pixel size (Å)	1.03									
Defocus range (μm)	1.5-3.0									
Electron dose (e^-/A^2)	25									
Reconstruction										
Software	FREALIGN	FREALIGN	RELION	RELION	RELION	RELION	RELION	RELION	RELION	RELION
Particles	15,779	2,276	177,642	132,076	149,628	83,102	11,107	25,580	106,640	80,783
Box size (pixels)	512^3	512^3	512^3	512^3	512^3	512^3	512^3	512^3	512^3	512^3
Symmetry imposed	I2	I2	C1	C1	C1	C1	C1	C1	C1	C1
Accuracy rotations (°)	0.14	0.18	0.15	0.16	0.16	0.19	0.35	0.25	0.17	0.18
Accuracy translations (pixels)	0.3	0.4	0.3	0.3	0.3	0.4	0.6	0.4	0.3	0.3
Map resolution (Å)	3.0	3.3	3.4	3.4	3.4	3.6	4.4	3.9	3.5	3.6
Map sharpening b-factor ($Å^2$)	-150	-120	-130	-120	-115	-125	-70	-120	-120	-120
Coordinate refinement										
Software	PHENIX	PHENIX	PHENIX	PHENIX	PHENIX	PHENIX	Not refined	PHENIX	PHENIX	PHENIX
Resolution cutoff (Å)	3.0	3.3	3.4	3.4	3.4	3.6	-	3.9	3.5	3.6
Resolution (Å, FSC = 0.5)	3.1	3.4	3.4	3.4	3.5	3.7	-	4.0	3.6	3.7
Model										
Number of residues	1051#	1051#	3915	4523	4523	4523	-	6332	8162	7554
B-factors overall	37.3	69.9	43.0	64.6	60.8	62.8	-	109.7	52.1	69.0
R.m.s. deviations										
Bond lengths (Å)	0.009	0.009	0.008	0.007	0.007	0.007	-	0.010	0.008	0.009
Bond angles (°)	1.200	1.216	1.213	1.141	1.130	1.149	-	0.975	0.859	1.019

Table S1 (continued)

	Large Shell (main population)	Compacted Shell	BMC-T^S large shell	BMC-T^D large shell closed inside	BMC-T^D large shell widened inside	BMC-T^D small shell open inside	Large shell C1 refinement	Four positions: BMC-$T^DT^ST^ST^S$	Four positions: BMC-$T^DT^DT^DT^D$	Four positions: BMC-$T^ST^DT^DT^D$
Validation										
Molprobity clashscore	5.7	5.1	6.8	6.6	7.2	5.4	-	7.6	6.1	2.2
Rotamer outliers (%)	0.0	0.17	0.04	0.03	0.34	0.06	-	0.3	0.2	0.0
C_β deviations (%)	0.0	0.0	0.0	0.0	0.0	0.0	-	0.0	0.0	0.0
Ramachandran plot										
Favored (%)	97.1	95.6	97.9	97.5	96.8	98.0	-	94.8	96.7	97.3
Allowed (%)	2.9	4.1	2.1	2.5	3.2	2.0	-	5.3	3.3	2.7
Outliers (%)	0.0	0.0	0.0	0.0	0.0	0.0	-	0.0	0.0	0.0

[#] one asymmetric unit